Inorganic Chemistry

pubs.acs.org/IC

Article

Selective Lanthanide Sensing with Gold Nanoparticles and Hydroxypyridinone Chelators

Roger M. Pallares, Korey P. Carter, Steven E. Zeltmann, Toni Tratnjek, Andrew M. Minor, and Rebecca J. Abergel*

Cite This: *Inorg. Chem.* 2020, 59, 2030−2036

Read Online

ACCESS | Metrics & More | Article Recommendations | Supporting Information

ABSTRACT: The octadentate hydroxypyridinone chelator 3,4,3-LI(1,2-HOPO) is a promising therapeutic agent because of its high affinity for f-block elements and noncytotoxicity at medical dosages. The interaction between 3,4,3-LI(1,2-HOPO) and other biomedically relevant metals such as gold, however, has not been explored. Gold nanoparticles functionalized with chelators have demonstrated great potential in theranostics, yet thus far, no protocol that combines 3,4,3-LI(1,2-HOPO) and colloidal gold has been developed. Here, we characterize the solution thermodynamic properties of the complexes formed between 3,4,3-LI(1,2-HOPO) and Au^{3+} ions and demonstrate how under specific pH conditions the chelator promotes the growth of gold nanoparticles, acting as both reducing and stabilizing agent. 3,4,3-LI(1,2-HOPO) ligands on the nanoparticle surface remain active and selective toward f-block elements, as evidenced by gold nanoparticle selective aggregation. Finally, a new colorimetric assay capable of reaching the detection levels necessary for the quantification of lanthanides in waste from industrial processes is developed based on the inhibition of particle growth by lanthanides.

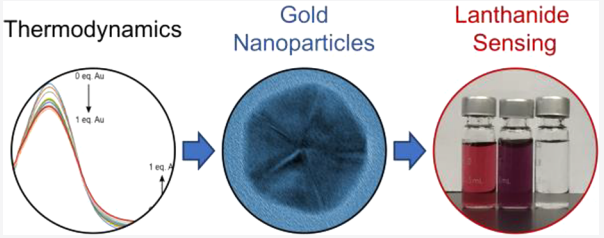

INTRODUCTION

Siderophores are a group of biomolecules produced by bacteria, fungi, and some plants that transport iron across cell membranes.[1] Bioinspired siderophore analogues that contain hydroxypyridinone (HOPO) groups, such as 3,4,3-LI(1,2-HOPO), are known for their high affinity for f-block cations.[2,3] As 3,4,3-LI(1,2-HOPO) can be orally administered and is noncytotoxic at medical dosages, it is primarily developed as a chelating agent for the decorporation of radionuclides and as a treatment for heavy metal poisoning.[4,5] In addition, the high stability and fast excretion kinetics of HOPO complexes with alpha-emitting isotopes have resulted in the pursuit of new radiopharmaceutical agents for cancer therapy,[6] and HOPO moieties are also known to sensitize the luminescence of several lanthanides, which can be applied to bioassays.[7−9] While the coordination chemistry of 3,4,3-LI(1,2-HOPO) with f-block cations has been thoroughly investigated,[2,3,7,8] the complexation of noble metals such as gold and their applications have yet to be explored.

Gold has been used in medicine throughout history from dentistry to arthritis treatment.[10] When the dimensions of metallic gold are reduced to the nanoscale, such as in the form of gold nanoparticles (AuNPs), different size- and shape-dependent physicochemical properties arise.[11−16] Because AuNP optical properties are sensitive to the particle surroundings, they can be used as transducers for sensitive bioassays.[17−23] Several chelating agents have been functionalized on the AuNP surface for the development of therapeutics and sensing agents;[24,25] however, the functionalization of chelators on AuNPs usually requires tedious multistep reactions.[24,25] Simultaneous one-pot synthesis and functionalization of AuNPs with chelating agents is a preferred approach, yet this has only been successful with a limited suite of ligands, including ethylenediaminetetraacetic acid (EDTA).[26] A method that combines the one-pot synthesis and functionalization of AuNPs with a better performing chelator, specifically for f-block elements such as 3,4,3-LI(1,2-HOPO), would be beneficial for the development of new nanoconstructs for biomedical applications.

In this work, we report a systematic study of the solution affinity of Au^{3+} and the therapeutic chelating agent 3,4,3-LI(1,2-HOPO). Au^{3+} complexation was observed even at acidic pH (2.2), where most of the HOPO binding units were protonated. Therefore, only a small fraction of partially deprotonated 3,4,3-LI(1,2-HOPO) was necessary to trigger complexation, indicative of a high thermodynamic stability between the cation and the chelator. Above pH 2.4, complexation was followed by the reduction of Au^{3+} to Au^0 and subsequent formation of AuNPs. During the growth of the particles, 3,4,3-LI(1,2-HOPO) acts as both reducing and

Received: November 19, 2019
Published: January 23, 2020

https://dx.doi.org/10.1021/acs.inorgchem.9b03393
Inorg. Chem. 2020, 59, 2030−2036

stabilizing agent. The competition between Au^{3+} and cations with higher binding affinities was used as sensing principle to quantify lanthanide concentrations in aqueous solutions. The tunable dynamic range of the colorimetric assay covers a wide range of concentrations relevant to the detection of lanthanides in waste from industrial processes.

RESULTS AND DISCUSSION

Complexation of Au^{3+} by 3,4,3-LI(1,2-HOPO). The interaction between Au^{3+} and 3,4,3-LI(1,2-HOPO) (Figure 1a) was initially studied at pH 2.2 because the chelator has

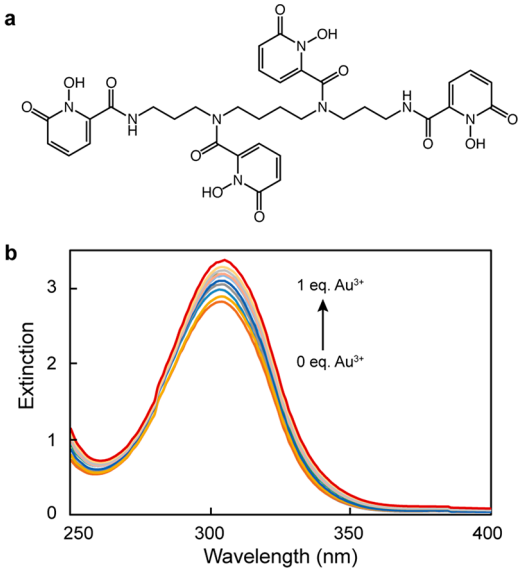

Figure 1. Solution thermodynamics between Au^{3+} and 3,4,3-LI(1,2-HOPO). (a) Structure of the chelator. (b) Spectrophotometric titration for the Au^{3+}-3,4,3-LI(1,2-HOPO) complex. The concentration of ligand was 400 μM, and the concentration of Au^{3+} ranged from 0 to 400 μM. The pH of the solution was 2.2 with an ionic strength of 0.1 M (KCl).

shown different complexation behaviors (from total binding to no interaction) with several metals at this acidic pH.[2,5] 1,2-HOPO chromophores have an extinction band at 303 nm, which is sensitive to metal binding;[2,5] thus, the complexation of Au^{3+} was studied by spectrophotometric titration from 250 to 400 nm (Figure 1b). The addition of one equivalent of Au^{3+} to a solution of 3,4,3-LI(1,2-HOPO) increased the intensity of the chelator band by 10 ± 2%, indicating formation of the complex. Two isosbestic points at 281 and 327 nm were observed (Figure 1b), which suggested that only two species, such as 3,4,3-LI(1,2-HOPO) and Au^{3+}, formed the complex.[27] The proton independent stability constants (i.e. equilibrium constants for the formation of complexes) between Au^{3+} and the chelator were determined via refinement of spectrophotometric titration data to be $\log \beta_{110} = 16.03 \pm 0.04$ for the $[Au\text{-}3,4,3\text{-}LI(1,2\text{-}HOPO)]^-$ complex and $\log\beta_{111} = 17.98 \pm 0.04$ for the [Au-3,4,3-LI(1,2-HOPO)H] complex (Table S1). The $\log \beta_{110}$ value is smaller than the corresponding stability constants reported for lanthanides (ranging from 16.4 to 22.2),[28] which are harder trivalent cations (weakly polarizable) that form more stable complexes with the HOPO chelator.

Since 3,4,3-LI(1,2-HOPO) binding affinities to cations are sensitive to the protonation of the 1,2-HOPO subunits (pK_a values ranging from 3.9 to 6.6),[7] the interaction between the ligand and Au^{3+} was further studied at varying pH values (Figure 2). Au^{3+} can be reduced to Au^0 at acidic pH (from 2.0

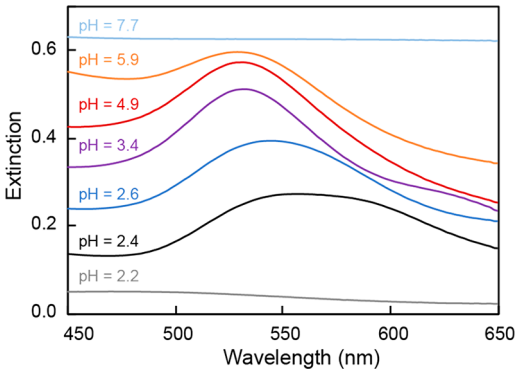

Figure 2. UV−vis of 1:1 mixtures of Au^{3+} and 3,4,3-LI(1,2-HOPO) at different pH values. The concentration of ligand and Au^{3+} was 400 μM in 100 μL of solution. The UV−vis spectra have been offset for clarity.

to 6.0) by nitrogen-rich molecules,[29,30] and as a result, the UV−vis spectra of the samples were measured from 450 to 650 nm, where colloidal Au absorbs.[11] The pH of the samples was adjusted prior to the addition of Au^{3+} with hydrogen chloride or sodium hydroxide, and the cation and chelator were left to react for 1 h. At pH 2.2, no extinction band between 450 and 650 nm was observed because Au^{3+} was complexed by 3,4,3-LI(1,2-HOPO), as described in the previous paragraph, and no reduction occurred. As the pH was systematically increased up to 5.9, an extinction band between 526 and 560 nm appeared, which correlates to the localized surface plasmon (LSP) resonances of AuNPs.[31] The LSP band was broad at low pH (from 2.4 to 3.4), indicating particle aggregation and/or polydispersity. As the pH increased up to 4.9, the LSP band centered at 526 nm and became sharper, which suggested the formation of monodisperse and well-dispersed AuNPs. At higher pH values, larger fractions of HOPO moieties are deprotonated, thereby providing stronger electrostatic repulsion between particles that favor AuNP dispersion. The system was further characterized by cyclic voltammetry (Figure S1) under AuNP growth conditions (pH 5.9). As nanoparticles start forming and depositing on the electrode at this pH, affecting the measurements, the solutions were mixed and left to stabilize for only 5 min before voltammetry measurements were performed. A positive half-wave potential (i.e. difference between cathodic and anodic peaks, $E_{1/2}$) of 0.685 V was measured, indicating that the reaction is thermodynamically favorable. The growth of AuNPs within this pH range (from 2.4 to 5.9) is consistent with the synthesis of particles made with other reducing agents.[7] Further increases of pH diminished the intensity of LSP band until total disappearance at pH 7.7. The lack of AuNP growth at higher pH was not caused by the formation of Au hydroxides as the speciation diagram calculated with the stability constants show that Au^{3+} and Au^{3+}-3,4,3-LI(1,2-HOPO) complexes are the primary species in solution between pH 1 and 10 (Figure S2).

Characterization of AuNPs. We chose to study the AuNPs synthesized at pH 4.9 because their UV−vis spectrum indicated they were primarily monodisperse in solution (Figure 3a). Scanning transmission electron microscope (STEM) images in dark field mode showed quasi-spherical AuNPs with average diameters of 24 ± 4 nm and a small fraction with

https://dx.doi.org/10.1021/acs.inorgchem.9b03393
Inorg. Chem. 2020, 59, 2030−2036

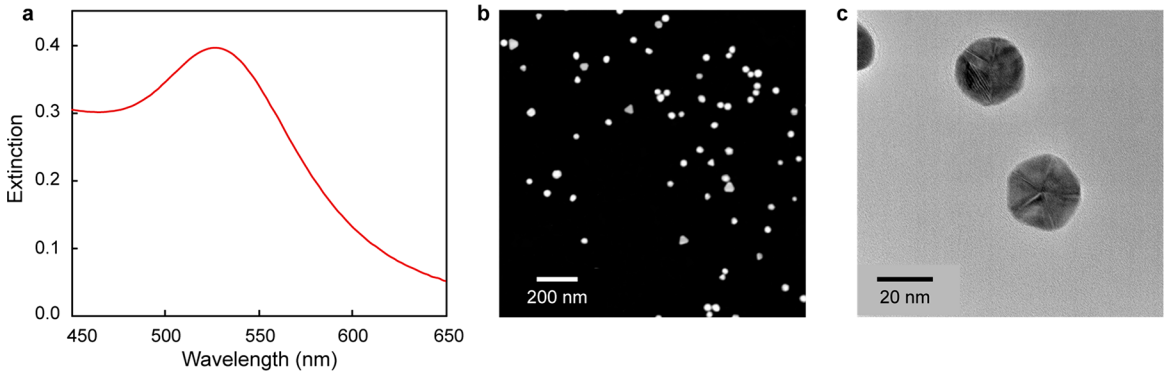

Figure 3. Characterization of AuNPs grown with 3,4,3-LI(1,2-HOPO) at pH 4.9. (a) UV−vis spectrum, (b) STEM image, and (c) HR-TEM image of AuNPs.

triangular shapes (Figure 3b and Figure S3). Both size dispersion (16.5%, calculated as percent of standard deviation) and crystal structure (the particles were polycrystalline with multiply twinned structures, Figure 3c and Figure S4) were very similar to the ones obtained via the Turkevich method by citrate reduction of gold salts.[32,33] Spectral analysis and mapping through the energy-dispersive X-ray spectroscopy (EDS) mode of the STEM confirmed that the NPs were made of Au (Figure S5). The yield of the particle synthesis defined as percentage of Au^{3+} that was reduced to metal and formed AuNP was 87.2% (a description of yield calculations is provided in the Experimental Section), consistent with well-established protocols.[34] A zeta potential value of −22.9 ± 2.6 mV was recorded after washing the particles and resuspending them in Milli-Q water (Table S2). The negative zeta potential of the particles confirmed their stability in solution, which was corroborated by the invariability of the LSP band after one month (Figure S6), suggesting that the chelator acted as stabilizing agent. The presence of the 3,4,3-LI(1,2-HOPO) on the metal surface was confirmed by fluorescence spectroscopy, exploiting the chelator sensitization properties. The complex formed between 3,4,3-LI(1,2-HOPO) and Eu^{3+} has a characteristic emission band centered at 618 nm,[7] which was recorded after the addition of $EuCl_3$ to the washed particle solution (Figure S7a). The addition of Eu^{3+} also caused the aggregation of the particles, as observed in their UV−vis spectrum (Figure S7b). Although AuNPs can quench the emission of fluorophores located on their surface, fluorescence enhancement occurs when the particles are aggregated because of the formation of hotspots.[35] Hence, the chelator acted as both reducing and stabilizing agent in the growth of the particles. The dual role of 3,4,3-LI(1,2-HOPO) is consistent with the synthesis of AuNPs with other chelates such as EDTA.[26] We confirmed by AuNP aggregation assay that the 3,4,3-LI(1,2-HOPO) on the Au surface preserved selectivity toward f-block elements over lighter ones as only lanthanides induced nanoparticle aggregation (Figure S8).

To further understand the growth mechanism of the particles, we tested the growth kinetics by UV−vis spectroscopy (Figure 4). An extinction band below 500 nm, which is characteristic of Au^0 interband transitions,[36] appeared in the first min after the addition of Au^{3+} to the growth solution, resulting in a faint red color visible by naked-eye within 5 min, and the extinction intensity of this band increased as the reaction progressed. After 18 min, a LSP band at 518 nm arose, which denoted the formation and growth of colloidal Au above 2 nm (size necessary to hold LSP resonances).[37] As the

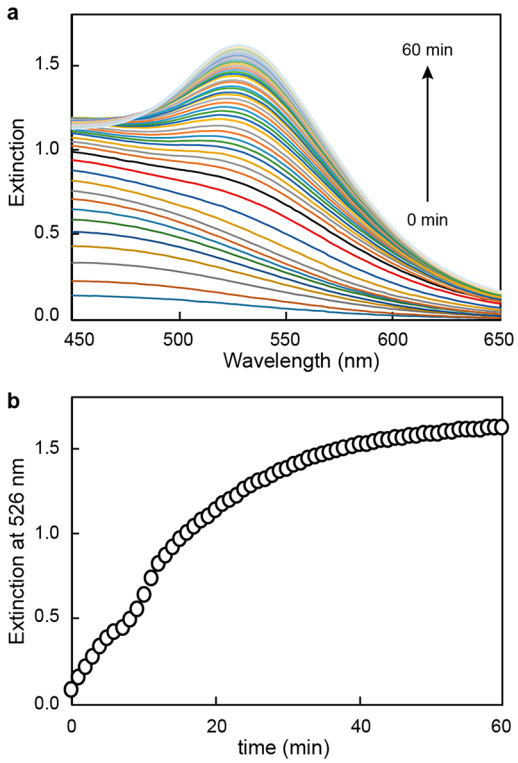

Figure 4. Growth kinetics of AuNPs at pH 4.9. (a) UV−vis spectra and (b) extinction variation at 526 nm during particle growth. The concentration of ligand and Au^{3+} was 400 μM in 1 mL of growth solution.

reaction continued, the LSP increased in intensity and shifted to 526 nm, suggesting particle growth. The reaction ended after 50 min when the position and intensity of the LSP band had stabilized.

Competition Experiments. As the interaction between Au^{3+} and 3,4,3-LI(1,2-HOPO) resulted in both complex formation and particle growth, we studied whether chelation of Au^{3+} was necessary to synthesize AuNPs or whether both events were independent. We performed a competition experiment with Eu^{3+}, whose thermodynamic stability constant with 3,4,3-LI(1,2-HOPO) is higher (log β_{110} of 20.2)[7] than the one we determined for Au^{3+}. It was previously shown that the complexation of Eu^{3+} by 3,4,3-LI(1,2-HOPO) occurs within 10 min;[8] thus, Eu^{3+} was added to the solution and allowed to interact with the chelate for 10 min prior the addition of Au^{3+}.

https://dx.doi.org/10.1021/acs.inorgchem.9b03393
Inorg. Chem. 2020, 59, 2030−2036

After Au^{3+} addition, the mixture was left to react for 1 h and then characterized by UV−vis spectroscopy. Figure 5a shows

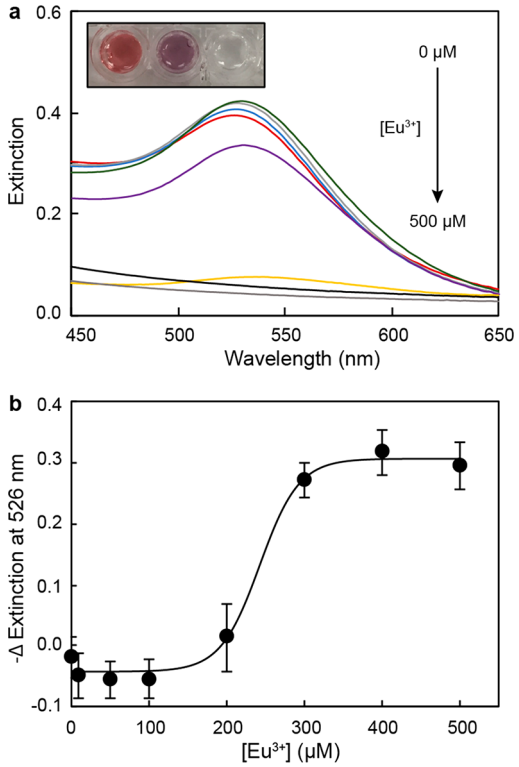

Figure 5. Competition experiments with Eu^{3+}. (a) UV−vis spectra of AuNPs grown after addition of Eu^{3+}. The final volume of the solutions was 100 μL. The inset is the picture of AuNP solution grown in the presence of 0, 200, and 400 μM Eu^{3+}. (b) Variation of the extinction intensity at LSP band maxima (526 nm) under different concentrations of Eu^{3+}.

that increasing the concentration of Eu^{3+} prevented the formation AuNPs as the LSP band decreased in intensity and red-shifted. This confirmed that the reduction of Au^{3+} to Au^0 by 3,4,3-LI(1,2-HOPO) required the complexation of Au^{3+} because the presence of a cation with higher affinity for the chelator hindered the particle growth, and these results were consistent with a previous publication that observed the reduction of hexavalent cations after being complexed by 3,4,3-LI(1,2-HOPO).[38] The variations in the LSP band due to the presence of Eu^{3+} during AuNP formation were examined as colorimetric sensing principle, where the color change of the solution could be used to quantify the analyte concentration (Figure 5b). Although lanthanides are usually quantified by ICP-MS and ICP-OES, these instruments are intensive in cost and personnel. Thus, a rapid and straightforward assay capable of quantifying lanthanide concentrations with minimal instrumentation or simply by naked-eye would be highly beneficial. Conventional colorimetric assays based on AuNP aggregation (Figure S8) only change in color as the concentration of analyte increases; the one presented in Figure 5, however, shows simultaneous color change (shift of the LSP band) and color disappearance (decrease of LSP intensity), which provide a more distinguishable analytical response, particularly when used as a point-of-care assay read by the naked-eye. The quantification accuracy was 87% (Table S3), which was estimated by analyzing a reference sample (250 μM Eu^{3+}), and it was similar to other nanoparticle-based colorimetric assay accuracies.[39] As a result, we explored the quenching of AuNP growth as a sensing principle with other lanthanides such as La^{3+}, Gd^{3+}, and Tb^{3+}, which also have thermodynamic stability constants with 3,4,3-LI(1,2-HOPO) higher than that with Au^{3+}.[2] As controls, we used Ca^{2+} and Cu^{2+}, two divalent cations commonly found in buffers that are softer than Au^{3+} and are expected to have a lower affinity for the chelator. The binding curves showed similar responses for all lanthanides (Figure 6), while Ca^{2+} and Cu^{2+} did not induce any significant changes as they did not prevent the formation of AuNPs.

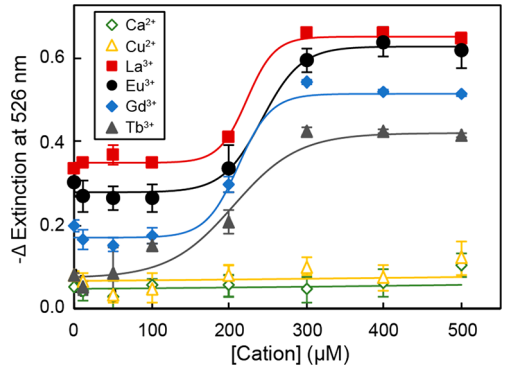

Figure 6. Colorimetric response for different metals. The concentration of ligand and Au^{3+} was 400 μM. The binding curves have been offset for clarity.

The United States Department of Energy (DOE) has highlighted the lanthanides as critical materials for clean energy technologies with high risk of supply disruptions in the near future.[40] Hence, new strategies to quantify and recycle rare-earth elements in waste streams are required.[40] One major challenge when characterizing lanthanides in solution is their wide concentration variations depending on the sample (i.e. from low to high micromolar or millimolar range in high level waste waters from nuclear reactors).[41] To take full advantage of a colorimetric assay, tunable limits of detection and dynamic ranges are necessary. Toward this goal, we adjusted both the limit of detection and the dynamic range by changing the concentration of chelate and Au^{3+}. Figure 7 depicts the colorimetric response at five different concentrations (from 100 to 600 μM $HAuCl_4$ and 3,4,3-LI(1,2-HOPO)). The limit of detection shifted from 3 to 302 μM as the concentrations of

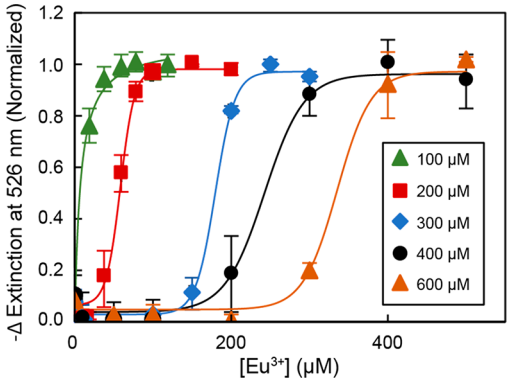

Figure 7. Colorimetric assay with tunable dynamic range. The response curve of the colorimetric assay under different concentrations of Au^{3+} and 3,4,3-LI(1,2-HOPO).

https://dx.doi.org/10.1021/acs.inorgchem.9b03393
Inorg. Chem. 2020, 59, 2030−2036

Au^{3+} and chelator increased. Thus, the combination of the five solutions yielded a colorimetric assay capable of covering the content of several lanthanides in waste from industrial processes (e.g. 3.1 μM Tb^{3+}, 105 μM Gd^{3+}, and 148 μM Eu^{3+}).[41]

CONCLUSIONS

In summary, we characterized the interaction between the hydroxypyridinonate chelator 3,4,3-LI(1,2-HOPO) and Au^{3+} in solution, where we observed ligand complexation of the cation even at acidic pH (2.2) when most of the HOPO binding units were protonated. As the pH increased, the formation of the complex was followed by the reduction of Au^{3+} to Au^0. Monodisperse AuNPs were obtained at pH 4.9 with the 3,4,3-LI(1,2-HOPO) acting as both reducing and stabilizing agent. The inhibition of particle growth by lanthanides was used as a colorimetric sensing principle, and the dynamic range of the assay was tuned by varying the concentrations of Au^{3+} and 3,4,3-LI(1,2-HOPO), reaching the limits of detection (3 μM) necessary to quantify lanthanides in waste from industrial processes. Finally, because our protocol allows for the straightforward synthesis of AuNPs that feature a chelator with high affinity for f-block elements on the surface, we anticipate new opportunities in biosensing and therapeutics will follow.

EXPERIMENTAL SECTION

Materials. 3,4,3-LI(1,2-HOPO) was prepared and characterized as previously described.[42] Chloroauric acid 99.9%, citric acid, disodium phosphate, lanthanum(III) chloride 99.9%, europium(III) chloride hexahydrate 99.99%, gadolinium(III) chloride hexahydrate 99%, terbium(III) chloride hexahydrate 99.9%, calcium chloride, copper(II) chloride 97%, 2-(*N*-morpholino)ethanesulfonic acid (MES), nitric acid (70%), and sodium hydroxide 97% were purchased from Sigma-Aldrich (St. Louis, MO). Hydrogen chloride 0.1 and 6 N was bought from VWR International (Radnor, PA). All solutions were prepared with Milli-Q water.

Spectrophotometric Titrations. Varying amounts of $HAuCl_4$ (from 0 to 1 equiv) were added to a set of solutions containing 3,4,3-LI(1,2-HOPO) kept at pH 2.2 with the addition of HCl, and an ionic strength of 0.1 M (KCl). The final volume of the solutions was 100 μL with a ligand concentration of 400 μM. The solutions were mixed for 10 s after the addition of Au^{3+} and incubated at room temperature without stirring for 1 h before recording UV−vis spectra from 250 to 400 nm with a SpectraMax iD3Multi-Mode Microplate Reader (Molecular Devices, Sunnyvale, CA).

Titration Data Treatment. Titration data were analyzed by nonlinear least-squares refinement with HypSpec software.[43] Equilibrium constants were defined as cumulative formation constants (β_{mlh}) based on eqs 1 and 2, where metal, ligand, and protons are described as M, L, and H, respectively.

$$mM + lL + hH \rightleftharpoons [M_mL_lH_h] \quad (1)$$

$$\beta_{mlh} = \frac{[M_mL_lH_h]}{[M]^m[L]^l[H]^h} \quad (2)$$

The h value for hydroxides was defined as negative. Based on previous studies,[5,6,44] all species formed with 3,4,3-LI(1,2-HOPO) were considered to have observable absorbance and were included in the data refinement. The chemical equilibria included in the constant calculations were water autoprotolysis, ligand protonation, ligand−metal complex formation, and metal hydroxide formation. The stability constants used during the refinement process are included in Table S1. The speciation diagram was calculated using the Hyperquad Simulation and Speciation (HYSS) software.[45]

Growth of AuNPs with 3,4,3-LI(1,2-HOPO). AuNPs were synthesized by adding 1 equiv of $HAuCl_4$ to 3,4,3-LI(1,2-HOPO) solutions (400 μM final concentration). The pH of the solutions was adjusted with hydrogen chloride or sodium hydroxide prior to the addition of Au^{3+}. The resulting solutions were mixed for 10 s and left undisturbed at room temperature for 1 h.

One-hundred microliters of the AuNP solutions was used to record UV−vis spectra with a SpectraMax iD3Multi-Mode Microplate Reader. Transmission electron microscopy (TEM) was performed using a FEI ThemIS (Thermo Fisher Scientific, Waltham, MA) with an image aberration corrector operated at 300 kV. AuNP morphology and elemental composition were characterized by high-angle annular dark field (HAADF) and energy dispersive spectroscopy (EDS) in STEM mode. High-resolution TEM (HR-TEM) micrographs were acquired on a FEI Ceta camera. Hydrodynamic diameter and zeta potential values were measured with a ZetaPlus BI-90 Plus (Brookhaven Instruments Corporation, Holtsville, NY).

To quantify the yield of the AuNP synthesis, the particles were washed by centrifugation (12 000 × g) for 15 min to remove unreacted Au^{3+} and redispersed in Milli-Q water. Fifty microliters of washed AuNPs were digested in 100 μL of nitric acid (70%) and 100 μL of hydrogen chloride (6 N) for 30 min at room temperature and redispersed in 4.75 mL of Milli-Q water, following previous published protocols.[46,47] The final concentration of Au in solution was quantified by inductively coupled plasma optical emission spectroscopy (ICP-OES, PerkinElmer, Waltham, MA).

Cyclic voltammetry (CV) data were collected at room temperature in water using 1 M of $CaCl_2$ as a supporting electrolyte with sweep rates of 50 mV/s over the range −200 to 1000 mV on a Pine Research (Durham, NC) WaveNow potentiostat. Gold ceramic screen-printed electrodes were used for CV measurements with a Ag/AgCl reference electrode, and the electrode surfaces were checked in between each measurement for potential deactivation using a 3 mM $Fe(CN)_6^{4-}$/$Fe(CN)_6^{3-}$ solution. CVs of blank solutions were also measured to subtract the influence of nonfaradic current; thus, all spectra presented herein are background subtracted.

Interaction between AuNPs and Cations. AuNPs were washed by centrifugation (12 000 × g) for 15 min to remove unreacted Au^{3+} and redispersed in MES buffer (0.1 M, pH 6.0). One microliter of cation solution was added to 100 μL of the AuNP solution, mixed, and incubated at room temperature for 10 min. The final concentration of cations was either 10 or 100 μM (the concentrations are described in the figure captions). The fluorescence and UV−vis spectra of solutions were recorded with a SpectraMax iD3Multi-Mode Microplate Reader.

Growth Kinetics of AuNPs. A 1 mL solution containing 400 μM of $HAuCl_4$ and 3,4,3-LI(1,2-HOPO) at pH 4.9 was prepared at room temperature and immediately transferred to a plastic cuvette. Solution state UV−vis spectra (from 450 to 650 nm) were recorded with a Cary 4000 UV−vis-NIR spectrophotometer (Agilent, Santa Clara, CA) at fixed intervals (one spectrum every min).

Competition Experiments. Solutions containing divalent (Ca^{2+} or Cu^{2+}) or trivalent (La^{3+}, Eu^{3+}, Tb^{3+}, or Gd^{3+}) cations were spiked into a set of 3,4,3-LI(1,2-HOPO) solutions at pH 4.9 and left to react for 10 min. Fixed amounts of $HAuCl_4$ were added into the mixtures for a final volume of 100 μL, where ligand and Au^{3+} concentrations were 400 μM, and the cation concentrations ranged from 0 to 1.25 equiv. The solutions were mixed after the addition of Au^{3+} and incubated at room temperature for 1 h before recording UV−vis spectra from 450 to 650 nm with a SpectraMax iD3Multi-Mode Microplate Reader. The measurement variation is reported as error bars in the figures, which represent one standard deviation of the measurements. For the tunable dynamic range experiments, the same protocol was followed, varying the amount of both 3,4,3-LI(1,2-HOPO) and $HAuCl_4$ in the growth solutions.

https://dx.doi.org/10.1021/acs.inorgchem.9b03393
Inorg. Chem. 2020, 59, 2030−2036

■ ASSOCIATED CONTENT

Supporting Information

The Supporting Information is available free of charge at https://pubs.acs.org/doi/10.1021/acs.inorgchem.9b03393.

Stability constants used in the data refinement or determined in the study, extinction variations at different wavelengths during spectrophotometric titration, speciation diagram for Au^{3+} and 3,4,3-LI(1,2-HOPO), size distribution of AuNPs, HR-TEM of AuNPs, elemental mapping of AuNPs grown with 3,4,3-LI(1,2-HOPO), stability studies of AuNPs, characterization of 3,4,3-LI(1,2-HOPO) on AuNP surface, and selectivity studies of chelate on AuNP surface (PDF)

■ AUTHOR INFORMATION

Corresponding Author

Rebecca J. Abergel − *Chemical Sciences Division, Lawrence Berkeley National Laboratory, Berkeley, California 94720, United States; Department of Nuclear Engineering, University of California, Berkeley, California 94720, United States;* orcid.org/0000-0002-3906-8761; Email: abergel@berkeley.edu

Authors

Roger M. Pallares − *Chemical Sciences Division, Lawrence Berkeley National Laboratory, Berkeley, California 94720, United States*

Korey P. Carter − *Chemical Sciences Division, Lawrence Berkeley National Laboratory, Berkeley, California 94720, United States;* orcid.org/0000-0003-4191-0740

Steven E. Zeltmann − *National Center for Electron Microscopy, Molecular Foundry, Lawrence Berkeley National Laboratory, Berkeley, California 94720, United States*

Toni Tratnjek − *Chemical Sciences Division, Lawrence Berkeley National Laboratory, Berkeley, California 94720, United States*

Andrew M. Minor − *National Center for Electron Microscopy, Molecular Foundry, Lawrence Berkeley National Laboratory, Berkeley, California 94720, United States; Department of Materials Science and Engineering, University of California, Berkeley, California 94720, United States*

Complete contact information is available at: https://pubs.acs.org/10.1021/acs.inorgchem.9b03393

Notes

The authors declare no competing financial interest.

■ ACKNOWLEDGMENTS

This work was supported by the Laboratory Directed Research and Development Program and by the U.S. Department of Energy (DOE), Office of Science, Office of Basic Energy Sciences, Chemical Sciences, Geosciences, and Biosciences Division, at the Lawrence Berkeley National Laboratory under Contract DE-AC02-05CH11231. SZ was supported by STROBE, a National Science Foundation Science & Technology Center under Grant No. DMR 1548924. The microscopy work was performed at the Molecular Foundry, a User Facility supported by the Office of Science, Office of Basic Energy Sciences, of the DOE under Contract DE-AC02-05CH11231.

■ REFERENCES

(1) Neilands, J. B. Siderophores: Structure and Function of Microbial Iron Transport Compounds. *J. Biol. Chem.* **1995**, *270* (45), 26723−26726.

(2) Deblonde, G. J. P.; Sturzbecher-Hoehne, M.; Abergel, R. J. Solution Thermodynamic Stability of Complexes Formed with the Octadentate Hydroxypyridinonate Ligand 3,4,3-LI(1,2-HOPO): A Critical Feature for Efficient Chelation of Lanthanide(IV) and Actinide(IV) Ions. *Inorg. Chem.* **2013**, *52* (15), 8805−8811.

(3) Sturzbecher-Hoehne, M.; Choi, T. A.; Abergel, R. J. Hydroxypyridinonate Complex Stability of Group (IV) Metals and Tetravalent f-Block Elements: The Key to the Next Generation of Chelating Agents for Radiopharmaceuticals. *Inorg. Chem.* **2015**, *54* (7), 3462−3468.

(4) Rees, J. A.; Deblonde, G. J. P.; An, D. D.; Ansoborlo, C.; Gauny, S. S.; Abergel, R. J. Evaluating the potential of chelation therapy to prevent and treat gadolinium deposition from MRI contrast agents. *Sci. Rep.* **2018**, *8* (1), 4419.

(5) Deblonde, G. J. P.; Lohrey, T. D.; An, D. D.; Abergel, R. J. Toxic heavy metal − Pb, Cd, Sn − complexation by the octadentate hydroxypyridinonate ligand archetype 3,4,3-LI(1,2-HOPO). *New J. Chem.* **2018**, *42* (10), 7649−7658.

(6) Deblonde, G. J. P.; Lohrey, T. D.; Booth, C. H.; Carter, K. P.; Parker, B. F.; Larsen, Å.; Smeets, R.; Ryan, O. B.; Cuthbertson, A. S.; Abergel, R. J. Solution Thermodynamics and Kinetics of Metal Complexation with a Hydroxypyridinone Chelator Designed for Thorium-227 Targeted Alpha Therapy. *Inorg. Chem.* **2018**, *57* (22), 14337−14346.

(7) Abergel, R. J.; D'Aléo, A.; Ng Pak Leung, C.; Shuh, D. K.; Raymond, K. N. Using the Antenna Effect as a Spectroscopic Tool: Photophysics and Solution Thermodynamics of the Model Luminescent Hydroxypyridonate Complex [EuIII(3,4,3-LI(1,2-HOPO))]−. *Inorg. Chem.* **2009**, *48* (23), 10868−10870.

(8) Daumann, L. J.; Tatum, D. S.; Snyder, B. E. R.; Ni, C.; Law, G.-l.; Solomon, E. I.; Raymond, K. N. New Insights into Structure and Luminescence of EuIII and SmIII Complexes of the 3,4,3-LI(1,2-HOPO) Ligand. *J. Am. Chem. Soc.* **2015**, *137* (8), 2816−2819.

(9) Ricano, A.; Captain, I.; Carter, K. P.; Nell, B. P.; Deblonde, G. J. P.; Abergel, R. J. Combinatorial design of multimeric chelating peptoids for selective metal coordination. *Chemical Science* **2019**, *10* (28), 6834−6843.

(10) Pricker, S. P. Medical uses of gold compounds: Past, present and future. *Gold Bull.* **1996**, *29* (2), 53−60.

(11) Eustis, S.; el-Sayed, M. a. Why gold nanoparticles are more precious than pretty gold: noble metal surface plasmon resonance and its enhancement of the radiative and nonradiative properties of nanocrystals of different shapes. *Chem. Soc. Rev.* **2006**, *35* (3), 209−217.

(12) Amendola, V.; Pilot, R.; Frasconi, M.; Maragò, O. M.; Iatì, M. A. Surface plasmon resonance in gold nanoparticles: a review. *J. Phys.: Condens. Matter* **2017**, *29* (20), 203002.

(13) Pallares, R. M.; Su, X.; Lim, S. H.; Thanh, N. T. K. Fine-tuning of gold nanorod dimensions and plasmonic properties using the Hofmeister effects. *J. Mater. Chem. C* **2016**, *4* (1), 53−61.

(14) Pallares, R. M.; Stilson, T.; Choo, P.; Hu, J.; Odom, T. W. Using Good's Buffers To Control the Anisotropic Structure and Optical Properties of Spiky Gold Nanoparticles for Refractive Index Sensing. *ACS Applied Nano Materials* **2019**, *2* (8), 5266−5271.

(15) Pallares, R. M.; Wang, Y.; Lim, S. H.; Thanh, N. T. K.; Su, X. Growth of anisotropic gold nanoparticles in photoresponsive fluid for UV sensing and erythema prediction. *Nanomedicine* **2016**, *11* (21), 2845−2860.

(16) Tepale, N.; Fernández-Escamilla, V. A. V.; Carreon-Alvarez, C.; González-Coronel, J. V.; Luna-Flores, A.; Carreon-Alvarez, A.; Aguilar, J. Nanoengineering of Gold Nanoparticles: Green Synthesis, Characterization, and Applications. *Crystals* **2019**, *9* (12), 612.

(17) Saha, K.; Agasti, S. S.; Kim, C.; Li, X.; Rotello, V. M. Gold nanoparticles in chemical and biological sensing. *Chem. Rev. (Washington, DC, U. S.)* **2012**, *112*, 2739−2779.

(18) Zeng, S.; Yong, K.-T.; Roy, I.; Dinh, X.-Q.; Yu, X.; Luan, F. A Review on Functionalized Gold Nanoparticles for Biosensing Applications. *Plasmonics* **2011**, *6* (3), 491.
(19) Pallares, R. M.; Kong, S. L.; Ru, T. H.; Thanh, N. T. K.; Lu, Y.; Su, X. A plasmonic nanosensor with inverse sensitivity for circulating cell-free DNA quantification. *Chem. Commun.* **2015**, *51* (77), 14524−14527.
(20) Pallares, R. M.; Thanh, N. T. K.; Su, X. Tunable plasmonic colorimetric assay with inverse sensitivity for extracellular DNA quantification. *Chem. Commun.* **2018**, *54* (80), 11260−11263.
(21) Pallares, R. M.; Bosman, M.; Thanh, N. T. K.; Su, X. A plasmonic multi-logic gate platform based on sequence-specific binding of estrogen receptors and gold nanorods. *Nanoscale* **2016**, *8* (48), 19973−19977.
(22) Li, N.; Su, X.; Lu, Y. Nanomaterial-based biosensors using dual transducing elements for solution phase detection. *Analyst* **2015**, *140* (9), 2916−2943.
(23) Sutarlie, L.; Ow, S. Y.; Su, X. Nanomaterials-based biosensors for detection of microorganisms and microbial toxins. *Biotechnol. J.* **2017**, *12* (4). DOI: 10.1002/biot.201500459
(24) Lisowski, C. E.; Hutchison, J. E. Malonamide-Functionalized Gold Nanoparticles for Selective, Colorimetric Sensing of Trivalent Lanthanide Ions. *Anal. Chem.* **2009**, *81* (24), 10246−10253.
(25) Rotz, M. W.; Culver, K. S. B.; Parigi, G.; MacRenaris, K. W.; Luchinat, C.; Odom, T. W.; Meade, T. J. High Relaxivity Gd(III)−DNA Gold Nanostars: Investigation of Shape Effects on Proton Relaxation. *ACS Nano* **2015**, *9* (3), 3385−3396.
(26) Diamai, S.; Negi, D. P. S. EDTA-capped gold nanoparticles as a colorimetric probe for aluminium. *Mater. Res. Express* **2016**, *3* (11), 115002.
(27) Moore, J. W.; Pearson, R. G.; Atwater, A. In *Kinetics and Mechanism*; John Wiley and Sons: New York, 1981; Chapter Experimental Methods and Treatment of Data.
(28) Sturzbecher-Hoehne, M.; Ng Pak Leung, C.; D'Aléo, A.; Kullgren, B.; Prigent, A.-L.; Shuh, D. K.; Raymond, K. N.; Abergel, R. J. 3,4,3-LI(1,2-HOPO): In vitro formation of highly stable lanthanide complexes translates into efficacious in vivoeuropium decorporation. *Dalton Trans.* **2011**, *40* (33), 8340−8346.
(29) Subramaniam, C.; Tom, R. T.; Pradeep, T. On the formation of protected gold nanoparticles from AuCl4−by the reduction using aromatic amines. *J. Nanopart. Res.* **2005**, *7* (2), 209−217.
(30) Chia, K.-K.; Cohen, R. E.; Rubner, M. F. Amine-Rich Polyelectrolyte Multilayer Nanoreactors for in Situ Gold Nanoparticle Synthesis. *Chem. Mater.* **2008**, *20* (21), 6756−6763.
(31) Jain, P. K.; Huang, X.; El-Sayed, I. H.; El-Sayed, M. A. Noble metals on the nanoscale: Optical and photothermal properties and some applications in imaging, sensing, biology, and medicine. *Acc. Chem. Res.* **2008**, *41* (12), 1578−1586.
(32) Wuithschick, M.; Birnbaum, A.; Witte, S.; Sztucki, M.; Vainio, U.; Pinna, N.; Rademann, K.; Emmerling, F.; Kraehnert, R.; Polte, J. r. Turkevich in New Robes: Key Questions Answered for the Most Common Gold Nanoparticle Synthesis. *ACS Nano* **2015**, *9* (7), 7052−7071.
(33) Kimling, J.; Maier, M.; Okenve, B.; Kotaidis, V.; Ballot, H.; Plech, A. Turkevich method for gold nanoparticle synthesis revisited. *J. Phys. Chem. B* **2006**, *110* (32), 15700−15707.
(34) Noruzi, M.; Zare, D.; Davoodi, D. A rapid biosynthesis route for the preparation of gold nanoparticles by aqueous extract of cypress leaves at room temperature. *Spectrochim. Acta, Part A* **2012**, *94*, 84−88.
(35) Horimoto, N. N.; Imura, K.; Okamoto, H. Dye fluorescence enhancement and quenching by gold nanoparticles: Direct near-field microscopic observation of shape dependence. *Chem. Phys. Lett.* **2008**, *467* (1), 105−109.
(36) Hartland, G. V. Optical Studies of Dynamics in Noble Metal Nanostructures. *Chem. Rev. (Washington, DC, U. S.)* **2011**, *111* (6), 3858−3887.
(37) Amendola, V.; Meneghetti, M. Size Evaluation of Gold Nanoparticles by UV−vis Spectroscopy. *J. Phys. Chem. C* **2009**, *113* (11), 4277−4285.
(38) Carter, K. P.; Jian, J.; Pyrch, M. M.; Forbes, T. Z.; Eaton, T. M.; Abergel, R. J.; de Jong, W. A.; Gibson, J. K. Reductive activation of neptunyl and plutonyl oxo species with a hydroxypyridinone chelating ligand. *Chem. Commun.* **2018**, *54* (76), 10698−10701.
(39) Wu, S.; Li, D.; Wang, J.; Zhao, Y.; Dong, S.; Wang, X. Gold nanoparticles dissolution based colorimetric method for highly sensitive detection of organophosphate pesticides. *Sens. Actuators, B* **2017**, *238*, 427−433.
(40) Chu, S. *Critical Materials Strategy*; US Department of Energy, 2010.
(41) Chitnis, R. R.; Wattal, P. K.; Ramanujam, A.; Dhami, P. S.; Gopalakrishnan, V.; Mathur, J. N.; Murali, M. S. Separation and Recovery of Uranium, Neptunium, and Plutonium from High Level Waste Using Tributyl Phosphate: Countercurrent Studies with Simulated Waste Solution. *Sep. Sci. Technol.* **1998**, *33* (12), 1877−1887.
(42) Abergel, R. J.; Durbin, P. W.; Kullgren, B.; Ebbe, S. N.; Xu, J.; Chang, P. Y.; Bunin, D. I.; Blakely, E. A.; Bjornstad, K. A.; Rosen, C. J.; Shuh, D. K.; Raymond, K. N. Biomimetic actinide chelators: an update on the preclinical development of the orally active hydroxypyridonate decorporation agents 3,4,3-LI(1,2-HOPO) and 5-LIO(Me-3,2-HOPO). *Health Phys.* **2010**, *99* (3), 401−407.
(43) Gans, P.; Sabatini, A.; Vacca, A. Investigation of equilibria in solution. Determination of equilibrium constants with the HYPERQUAD suite of programs. *Talanta* **1996**, *43* (10), 1739−1753.
(44) Deblonde, G. J. P.; Lohrey, T. D.; Abergel, R. J. Inducing selectivity and chirality in group IV metal coordination with high-denticity hydroxypyridinones. *Dalton Trans.* **2019**, *48* (23), 8238−8247.
(45) Alderighi, L.; Gans, P.; Ienco, A.; Peters, D.; Sabatini, A.; Vacca, A. Hyperquad simulation and speciation (HySS): a utility program for the investigation of equilibria involving soluble and partially soluble species. *Coord. Chem. Rev.* **1999**, *184* (1), 311−318.
(46) Yue, J.; Pallares, R. M.; Cole, L. E.; Coughlin, E. E.; Mirkin, C. A.; Lee, A.; Odom, T. W. Smaller CpG-Conjugated Gold Nanoconstructs Achieve Higher Targeting Specificity of Immune Activation. *ACS Appl. Mater. Interfaces* **2018**, *10* (26), 21920−21926.
(47) Pallares, R. M.; Choo, P.; Cole, L. E.; Mirkin, C. A.; Lee, A.; Odom, T. W. Manipulating Immune Activation of Macrophages by Tuning the Oligonucleotide Composition of Gold Nanoparticles. *Bioconjugate Chem.* **2019**, *30* (7), 2032−2037.